JOURNAL OF INFORMATION PROCESSING SYSTEMS JIPS

Blind Image Quality Assessment on Gaussian Blur Images

Liping Wang*, Chengyou Wang*, and Xiao Zhou*

Abstract

Multimedia is a ubiquitous and indispensable part of our daily life and learning such as audio, image, and video. Objective and subjective quality evaluations play an important role in various multimedia applications. Blind image quality assessment (BIQA) is used to indicate the perceptual quality of a distorted image, while its reference image is not considered and used. Blur is one of the common image distortions. In this paper, we propose a novel BIQA index for Gaussian blur distortion based on the fact that images with different blur degree will have different changes through the same blur. We describe this discrimination from three aspects: color, edge, and structure. For color, we adopt color histogram; for edge, we use edge intensity map, and saliency map is used as the weighting function to be consistent with human visual system (HVS); for structure, we use structure tensor and structural similarity (SSIM) index. Numerous experiments based on four benchmark databases show that our proposed index is highly consistent with the subjective quality assessment.

Keywords

Blind Image Quality Assessment (BIQA), Gaussian Blur Image, Saliency Map, Structure Tensor, Structural Similarity (SSIM)

1. Introduction

With the rapid development of digital imaging and technology, large numbers of images are available in our daily life. In recent years, more and more people share images through the social network. Images play an important role in our communication and interaction with the world around us. However, the quality of an image is usually degraded by various distortions during acquisition and processing [1]. For example, the visual quality of image captured is poor under poor weather conditions or by low end devices.

The purpose of image quality assessment (IQA) is to measure the image quality using models that is consistent with the subjective evaluation. Therefore, it can be used to evaluate the performance of image processing systems, and thus help to select the optimal parameters in image processing. It is useful in many applications, such as image watermarking [2] and image enhancement [3]. To this end, various IQA methods have been proposed. According to the usage of the reference image, objective IQA metrics can be divided into three categories: full reference (FR) [4,5], reduced-reference (RR) [6], and blind/no-reference (NR) [7].

In general, the reference image is not available in most cases. Therefore, blind/no-reference image quality assessment (NR-IQA) is more practical. The intent of NR-IQA is to design computational models that can indicate the quality of distorted images without any prior information with respect to the original images. Some NR-IQA algorithms utilize natural scene statistics (NSS). The NSS-based NR-IQA algorithms can be classified into spatial domain method [8] and transform domain method [9]. The method based on the learned regression model is another category of NR-IQA algorithms [10].

Blur is one of the common distortions in image processing. The capturing of an image can cause image blurring, such as out-of-focus. Image manipulation procedures can also produce image blurring, such as image compression. To improve the quality of the compressed image, some image algorithms are used to remove noise or compression artifacts. However, most of the corrections use low-pass filters. They smooth artifacts, but lead to blurring effect.

To control and quantify the blurring effect, many blur metrics based on edge detection have been proposed. Marziliano et al. [11] first used Sobel operator to detect image edges. Cao et al. [12] proposed a local blur measure to estimate blurring effect on each pixel along the image's edges. Because the most common cause of image sharpness degradation is blur, blurriness evaluation is often equated with sharpness assessment. Feichtenhofer et al. [13] provided sharpness metric by exploiting the local edges gradient. A spatial domain sharpness metric based on just noticeable blur (JNB) was proposed in [14]. Based on the idea of JNB, Narvekar and Karam [15] proposed the cumulative probability of blur detection (CPBD) to quantify the image sharpness. These methods are spatial domain. There are also many transform-domain blur metrics. Hassen et al. [16] analyzed the local phase coherence (LPC) and applied it in image sharpness assessment. In [17], a hybrid-domain approach was proposed and support vector machine (SVM) was used.

Different from pervious methods, we propose a novel blind blur image quality assessment method in this paper. The novel method is based on the fact that the image with different blur degree will have different changes through the same blur. We describe this discrimination from three aspects: color, edge, and structure. For color, the color histogram map is used to measure the difference of different images; for edge, we use edge intensity map, and saliency map is used as the weight of edge intensity map in order to correspond better to human subjective feelings; for structure, we use structure tensor to distinguish between smooth and non-smooth regions and structural similarity (SSIM) index [4] to calculate the difference of smooth regions. At last, three features are pooled into the final index.

The rest of this paper is organized as follows. Section 2 introduces the related work of this paper. Section 3 presents the proposed scheme. The experimental results and analysis are presented in Section 4. Finally, conclusion and further research are given in Section 5.

2. Related Work

2.1 Structure Tensor Theory

In the practical application of human vision, how the image can be better perceived by human eyes need to be focused firstly. Therefore, if we design a quality evaluation method which is suitable for human vision, it is necessary to consider how to match up with the human visual system (HVS).

When eyes observe an image, the stimulus of the image to human eyes is a combination of different

amplitudes and different frequency signals. The response of human eyes to stimulus is not only related to the stimulus but also other signals. The contrast masking feature is a phenomenon that human eyes in the presence of a visual stimulus would perceive changes of the other visual stimulus. Due to the existence of masking, some distortions in the image can be ignored by human eyes, which have little effect on the overall quality of the image, while some distortions will be enhanced.

Masking characteristics of the HVS show that the details of the image in an area of dramatic changes are not likely to be perceived by human eyes. Even if the change is too drastic, it can also be masked out. Therefore, using different weights can not only reflect the human visual masking characteristics in the local area, but also more accord with visual image evaluation of human eyes.

The blur process can be obtained by the original image after the Gaussian filter, and the bandwidth of the filter determines the blur degree of distorted images. Fig. 1 shows a series of Lena images with size of 512×512.

(a)   (b)   (c)

Fig. 1. Comparison of the original image and two blurred images: (a) original image, (b) blurred image, and (c) twice blurred image.

Fig. 1(a) is the original image and Fig. 1(b) is a blurred image which is produced by the Gaussian filter on Fig. 1(a). The Gaussian filter has the kernel with size of 11×11, and its mean and variance are 0 and 1.5, respectively. Fig. 1(c) is the twice blurred image which is produced on Fig. 1(b) using the same Gaussian filter. From Fig. 1, we can see that there are obvious differences between Fig. 1(a) and Fig. 1(b) in visual quality. However, there is a little difference between Fig. 1(b) and Fig. 1(c). Blur mainly affects the regions of images rich in edge and texture, and it has little effect on the quality of smooth regions in the image. Therefore, the measure of the blurred image is to calculate the effect of Gaussian filter on the regions of images rich in edge and texture.

The visual response of the human eyes to blur and noise distortion is very different. Image quality can be measured by calculating the degree of distortion in different regions of the image to make the evaluation results closer to the visual perception evaluation results. In this paper, we use the structure tensor [18] to distinguish different regions.

For an image $f(x, y)$, the structure tensor is based on the gradient of f:

$$f_x = g_{x,\sigma} * f \ , \ \ f_y = g_{y,\sigma} * f \ , \tag{1}$$

where $*$ is convolution. f_x and f_y are gradients. $g_{x,\sigma}$ and $g_{y,\sigma}$ are the spatial derivatives in x and y directions with standard deviation σ, respectively:

$$g_\sigma(x,y) = \frac{1}{\sqrt{2\pi}\sigma}\exp\left(-\frac{x^2+y^2}{2\sigma^2}\right). \tag{2}$$

The gradient tensor Q_σ will be obtained by calculating the Cartesian product of the gradient vector $(f_x, f_y)^{\mathrm{T}}$:

$$Q_\sigma = \begin{pmatrix} q_{11} & q_{12} \\ q_{21} & q_{22} \end{pmatrix} = \begin{pmatrix} f_x^2 & f_x f_y \\ f_x f_y & f_y^2 \end{pmatrix}. \tag{3}$$

The structure tensor is shown as Eq. (4):

$$S_{\sigma',\sigma} = (s_{ij}),\ s_{ij} = g_{\sigma'} * q_{ij},\ (i,j \in \{1,2\}), \tag{4}$$

where σ' is the scale of spatial averaging. Corner is measured by the strength of the intrinsically 2-D response, for example:

$$c_1 = \frac{\det(s_{\sigma',\sigma})}{\mathrm{tr}(s_{\sigma',\sigma})}\ \text{or}\ c_2 = \det(s_{\sigma',\sigma}) - 0.04[\mathrm{tr}(s_{\sigma',\sigma})]^2. \tag{5}$$

2.2 Structural Similarity Measure Theory

SSIM [4] is based on the assumption that images are highly structured, and HVS is sensitive to structural distortion. For two image blocks x and y, the SSIM computes their similarity from three components: luminance similarity $l(x,y)$, contrast similarity $c(x,y)$, and structural similarity $s(x,y)$. These three components are described as Eqs. (6)–(8), respectively:

$$l(x,y) = \frac{2\mu_x\mu_y + C_1}{\mu_x^2 + \mu_y^2 + C_1}, \tag{6}$$

$$c(x,y) = \frac{2\sigma_x\sigma_y + C_2}{\sigma_x^2 + \sigma_y^2 + C_2}, \tag{7}$$

$$s(x,y) = \frac{\sigma_{xy} + C_3}{\sigma_x\sigma_y + C_3}, \tag{8}$$

where μ_x and μ_y are the mean of x and y, respectively. σ_x^2 and σ_y^2 represent the variance of x and y, respectively. σ_{xy} is the covariance of x and y. C_1, C_2, and C_3 are small constants to keep the denominator from being zero.

The SSIM is given as:

$$\mathrm{SSIM}(x,y) = [l(x,y)]^\alpha [c(x,y)]^\beta [s(x,y)]^\gamma, \tag{9}$$

where α, β, and γ are weights of these three components. The higher the value of SSIM is, the more similar image blocks x and y are. If y and x are the same, then the SSIM will be 1.

3. Proposed Blind Image Quality Assessment Method

3.1 Basic Principle

The process of image blurring can be described by Eq. (10):

$$g(x,y) = i(x,y) * h(x,y) + n(x,y) \, , \tag{10}$$

where $*$ indicates convolution operation. $i(x, y)$ is the original image. $h(x, y)$ is the blurring point-spread function. $n(x, y)$ is the additive noise. $g(x, y)$ is the degraded image. Because the blurring effect is caused by a loss of the high frequency, we can use a low-pass filter to reproduce. We select one set of Monarch images with Gaussian blur distortion from LIVE database [19], as shown in Fig. 2. These Monarch images with different distortion levels are filtered by the same Gaussian low-pass filter with 7×7 filtering window, as shown in Fig. 3.

| | | |
| (a) | (b) | (c) |

Fig. 2. A series of Monarch images with different Gaussian blur levels in LIVE database: (a) img173, (b) img3, and (c) img11.

| | | |
| (a) | (b) | (c) |

Fig. 3. A series of Monarch images re-blurred with the same Gaussian filter: (a) img173, (b) img3, and (c) img11.

Comparing Fig. 2 with Fig. 3, we observe a high difference in terms of loss of details between Fig. 2(a) and Fig. 3(a), and a slight difference between Fig. 2(b) and Fig. 3(b). Fig. 2(c) and Fig. 3(c) are almost the same. We can find that the sharper the image is, the gray levels of neighboring pixels will change larger after the same blur operation. The key idea of our proposed method is to blur the initial image firstly, and then analyze the difference between the initial image and re-blurred image.

3.2 Algorithm Description of Blur Metric

From Figs. 2 and 3, the color contrast of blurred images decreases with the enhancement of blur degree. Fig. 4 represents color histograms of Figs. 2 and 3, respectively. From Fig. 4, we can see that the more blurred the images are, the slower the signal intensity changes. Comparing Fig. 4, we observe a high difference between Fig. 4(a) and 4(b), and a slight difference between Fig. 4(c) and 4(d). Fig. 4(e) and 4(f) are almost the same. This phenomenon is the same as the above. In order to describe the difference and quantitatively describe the characteristics of blurred images, this paper proposes a novel method. The detailed process of this method is as follows:
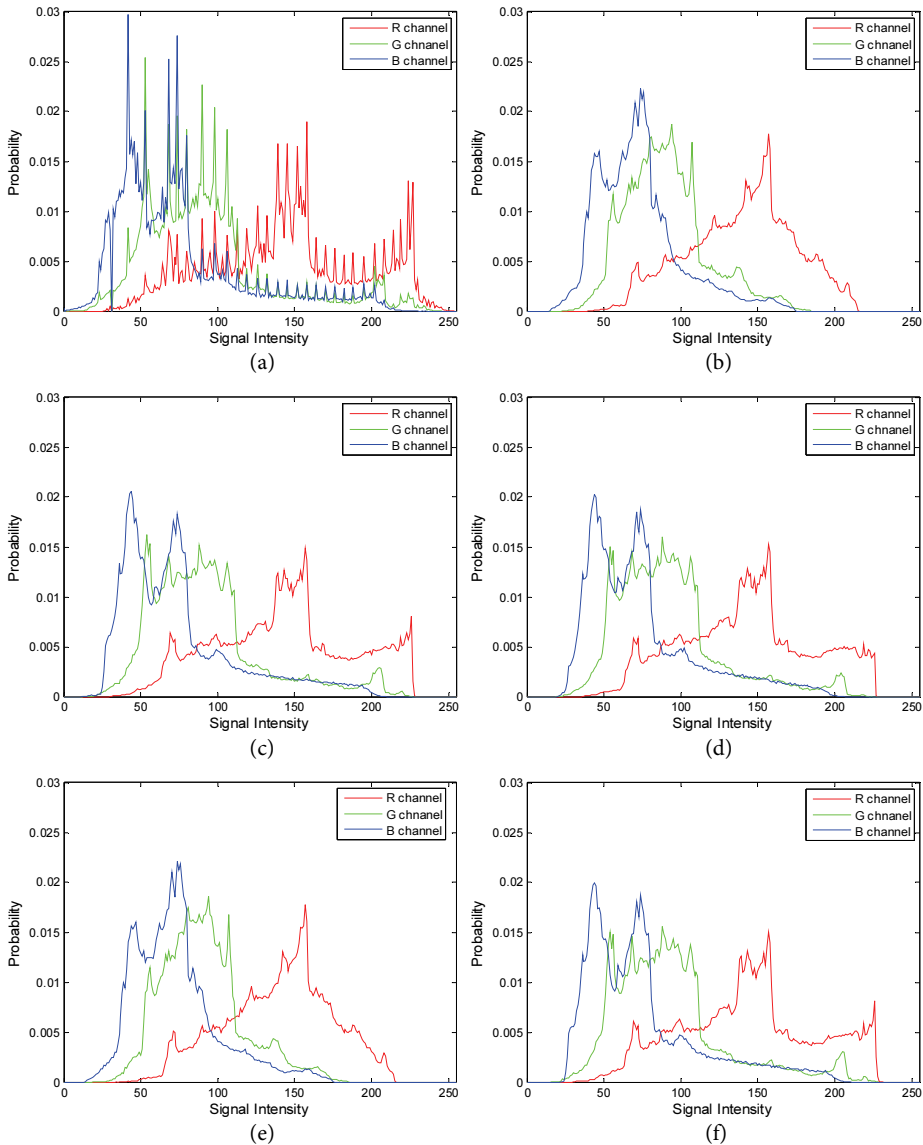

Fig. 4. Histograms maps of blurred images in Figs. 2 and 3: (a) img173, (b) re-blurred img173, (c) img3, (d) re-blurred img3, (e) img11, and (f) re-blurred img11 (that is, the left column corresponds to Fig. 2 and the right column corresponds to Fig. 3).

Step 1. Filter input image $f_1(x, y)$ (that is, image to be evaluated) by Gaussian filter and obtain re-blurred image $f_2(x, y)$;

Step 2. Calculate histograms of three color channels for input image $f_1(x, y)$ and re-blurred image $f_2(x, y)$, dubbed as H_1 and H_2, respectively;

Step 3. Calculate the absolute value of the difference between H_1 and H_2, and the sum of these changes, that is, $S_H = \sum |H_1 - H_2|$;

Step 4. A slight change of image is not easy to be detected. In order to avoid the cumulative effect of small changes in three color channels, the obtained score S_H is sorted in descending order, dubbed as S_{HD}. The sum of top 80% in S_H is the evaluation index for blurred image, that is, $S_{HDF} = \sum S_{HD}(1 : \text{round}(0.8L))$, where L represents the length of S_{HD}.

Another major feature of blurred image is that edges of blurred image are harder to detect. The regions of edges and texture in image are reduced, and the smooth regions become larger. Fig. 5 shows edge intensity maps of blurred images in Figs. 2 and 3, which are obtained by using Sobel edge detection operators. From Fig. 5(a)–(c), the more blurred the images are, the vaguer those edge intensity maps will be. If input images are more blurred, there are smaller differences in edge intensity maps between input images and re-blurred images. In order to quantitatively describe the characteristics of blurred images, this paper proposes S_E as shown in Eq. (11):

$$S_E = \frac{1}{m \cdot n \cdot l} \sum | D_1 - D_2 |, \tag{11}$$

where D_1 and D_2 are edge intensity maps of input image and re-blurred image, respectively. The image size is $m \times n$ pixels (vertical and horizontal pixels) and the number of color components is l. As for gray images, $l=1$, and for color images, $l=3$.
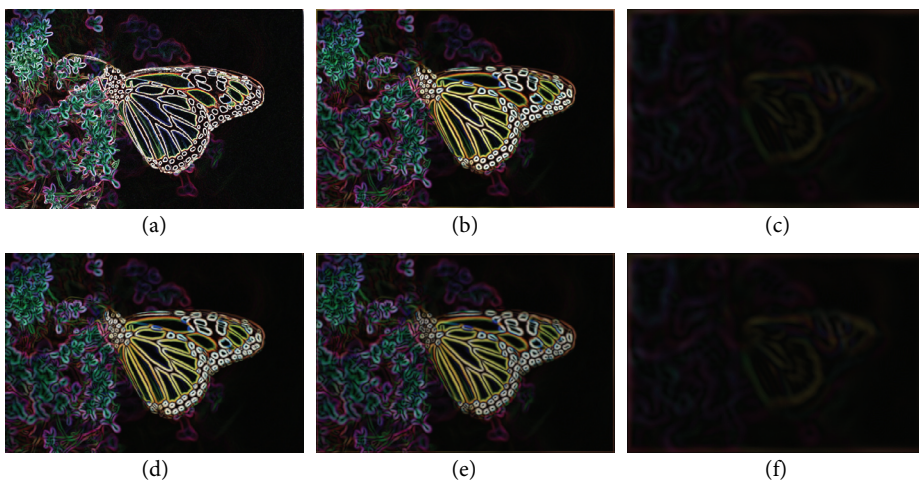

Fig. 5. Edge intensity maps of blurred images: (a) img173, (b) img3, (c) img11, (d) re-blurred img173, (e) re-blurred img3, and (f) re-blurred img11 (that is, the top row corresponds to Fig. 2 and the bottom row corresponds to Fig. 3).

Most vertebrates have a remarkable ability to automatically pay more attention to salient regions of the scene. Many scholars have widely studied that how to build effective computational models to imitate human visual attention [20]. The relationship between visual saliency and image quality assessment has been investigated by some researchers, and many approaches have been tried to integrate visual saliency into image quality assessment metric to potentially improve their prediction performance. To make our image quality assessment model more consistent with HVS, we use visual saliency map as a weighting function for calculating S_E. According to the research of Zhang et al. [21], we use the method proposed in [22] to calculate the visual saliency. Therefore, Eq. (11) is modified by visual saliency map, and the modified image blur quality metric S_{EF} is shown in Eq. (12):

$$S_{EF} = \frac{1}{m \cdot n \cdot l} \sum (M_{VS} \cdot | D_1 - D_2 |) , \tag{12}$$

where M_{VS} is visual saliency map.

As shown in Eq. (10), blurred image is produced by two parts: $i(x, y) * h(x, y)$ and $n(x, y)$. S_{HDF} and S_{EF} are calculated for the first part $i(x, y) * h(x, y)$ from color and edge intensity. For $n(x, y)$, people are more prone to perceive noise in smooth regions. Humans have a greater tolerance for the noise in the texture regions and edge regions. Considering this characteristic, this paper uses structure tensor to distinguish between smooth and non-smooth regions of the image and calculates the SSIM of smooth regions between input image and re-blurred image, dubbed as S_{SSIMT}. Fig. 6 shows smooth regions and non-smooth regions of blurred images where non-black regions indicate smooth regions and black regions indicate non-smooth regions. In this paper, these images are called as structure tensor maps. If S_{SSIMT} is smaller, the input image will be better. In fact, S_{SSIMT} can also be used as index for $i(x, y) * h(x, y)$, because a more blurred image has a higher similarity with its re-blurred image.
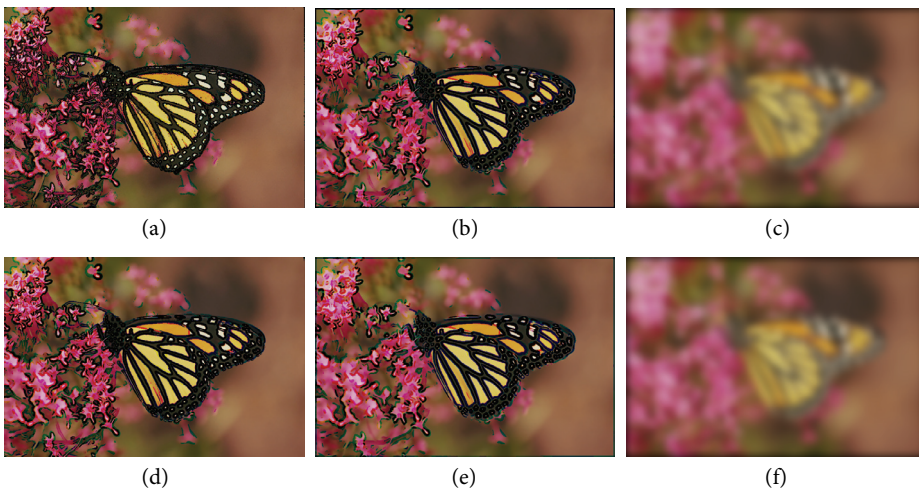

Fig. 6. Structure tensor maps of blurred images: (a) img173, (b) img3, (c) img11, (d) re-blurred img173, (e) re-blurred img3, and (f) re-blurred img11 (that is, the top row corresponds to Fig. 2 and the bottom row corresponds to Fig. 3).

With the color, edge intensity, and structure tensor features, we can define a novel method for blind quality assessment of blurred image. The input blurred image $f_1(x, y)$ is firstly pre-processed by Gaussian low-pass filter, and the re-blurred image $f_2(x, y)$ is obtained. We define the final score S as follows:

$$S = \alpha S_{HDF} + \beta S_{EF} - \lambda S_{SSIMT} \text{,}$$ (13)

where α, β, and γ are three parameters used to adjust the weights of color, edge intensity, and structure tensor features, respectively. This process can be illustrated by Fig. 7.
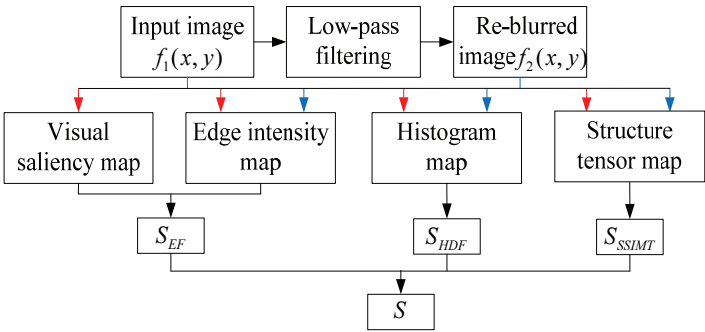

Fig. 7. The process of our proposed blind blur image quality assessment.

4. Experimental Results and Discussion

4.1 Datasets and Evaluation

Experiments were conducted on four large-scale image datasets, including TID2013 [23], TID2008 [24], CSIQ [25], and LIVE [19]. The important information of these four datasets was summarized in Table 1. For TID2013 database, 125 blurred images at 5 distinct levels were used in this study; for TID2008 database, 100 blurred images at 4 different levels were applied here; for CSIQ database, we picked 150 blurred images from this database for testing; for LIVE database, we adopted 174 images (including 29 source images and 145 blurred images). The subjective quality of the images in TID2013 and TID2008 is measured by mean opinion scores (MOS). In LIVE and CSIQ, the difference mean opinion score (DMOS) is used.

Table 1. Benchmark datasets for the experimentation

Datasets	Source images	Distorted images	Distortion types	Observers
TID2013	25	3000	25	971
TID2008	25	1700	17	838
CSIQ	30	866	6	35
LIVE	29	779	5	161

Four commonly used performance metrics are employed to evaluate our proposed method: Spearman rank-order correlation coefficient (SROCC), Kendall rank-order correlation coefficient (KROCC), Pearson linear correlation coefficient (PLCC), and root mean squared error (RMSE). A good method is expected to attain high values in SROCC, KROCC, and PLCC, as well as low values in RMSE. In this experiment, for calculating SROCC and KROCC, we use the proposed score and MOS/DMOS; for calculating PLCC and RMSE, we use MOS/DMOS and the proposed score after nonlinear regression. The nonlinear regression uses the following mapping function [26]:

$$f(x) = \beta_1 \left(\frac{1}{2} - \frac{1}{\exp(\beta_2(x - \beta_3))} \right) + \beta_4 x + \beta_5,$$ (14)

where β_i, $i=1,2,\dots,5$ are the parameters to be fitted.

4.2 Results and Discussion

We first conduct the image-level evaluation using our proposed method. We test our proposed method using four kinds of images which have different blur levels in LIVE database, as shown in Fig. 8. Fig. 8 only shows the four source images and the number in this experiment is 24, including the source images. For calculating S according to Eq. (13), we select $\alpha=1$, $\beta=1/20$, and $\gamma=1$. The blur scores generated by single feature and pooling feature are given in Table 2.

Table 2. Blur scores generated by single feature and pooling feature

| Test images		DMOS	S_{HDF}	S_{EF}	S_{SSIMT}	S
Monarch	img11	11.3333	0.0434	0.0344	0.9826	-0.9374
	img37	2.8541	0.1447	0.3490	0.8580	-0.6959
	img3	1.8515	0.2271	0.7181	0.7839	-0.5209
	img103	1.7083	0.2480	0.8214	0.7658	-0.4820
	img96	0.9062	0.3547	2.0615	0.5859	-0.1281
	img173	0.0000	0.8351	4.3802	0.3496	0.7045
Parrots	img69	7.6667	0.0575	0.0663	0.9690	-0.9082
	img105	4.0000	0.0775	0.1305	0.9425	-0.8585
	img31	2.1666	0.1001	0.3197	0.8753	-0.7592
	img56	1.2500	0.1299	0.8796	0.7528	-0.5789
	img12	0.7916	0.1619	1.7204	0.6035	-0.3555
	img154	0.0000	0.2881	3.6035	0.3274	0.1409
Woman-hat	img132	3.5416	0.1068	0.1583	0.9123	-0.7976
	img36	1.9375	0.1350	0.4689	0.8394	-0.6810
	img42	1.4791	0.1680	0.8022	0.747	-0.5365
	img61	1.0208	0.2205	1.5684	0.5717	-0.2728
	img82	0.6670	0.2736	2.7055	0.3988	0.0101
	img162	0.0000	0.4500	4.9183	0.2165	0.4794
Church-and-capitol	img104	7.6667	0.1090	0.1018	0.9625	-0.8484
	img66	1.5651	0.2756	1.4966	0.6655	-0.3151
	img91	1.2500	0.3226	2.3716	0.5745	-0.1334
	img2	0.9062	0.3944	4.1164	0.4414	0.1588
	img142	0.7343	0.4305	5.4987	0.3729	0.3325
	img172	0.0000	0.6042	11.3414	0.2212	0.9500
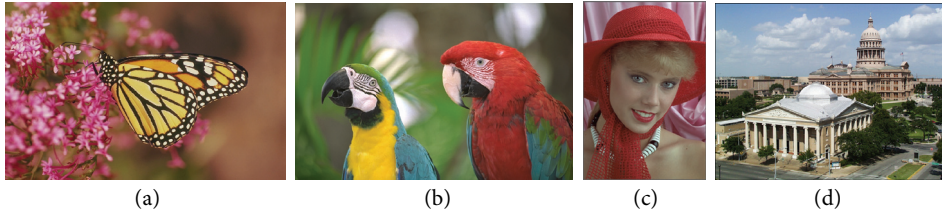
Fig. 8. Four kinds of images in image-level evaluation: (a) Monarch, (b) Parrots, (c) Woman-hat, and (d) Church-and-capitol.

In LIVE, a lower subjective score indicates a better image quality. From Table 2, the proposed method monotonically decreases blur scores S_{HDF} and S_{EF}, pooling score S, while monotonically increases blur score S_{SSIMT}. Humans have the capability to distinguish the blur degree independent of image content. If images have similar blur degree, we should give them similar blur scores. Compared img96 with img2, their DMOS scores are the same. Their S_{HDF} scores are 0.3547 and 0.3944. Their S_{EF} scores are 2.0615 and 4.1164. Their S_{SSIMT} scores are 0.5859 and 0.4414, and their S scores are -0.1281 and 0.1588. By observing distorted images in LIVE database, people can hardly distinguish the blur degree levels of "img91 & img2" and "img2 & img142". For img91, img2, and img142, their DMOS scores are 1.2500, 0.9062, and 0.7343, respectively. Correspondingly, the scores of the proposed method are -0.1334, 0.1588, and 0.3325, respectively. Compared with these differences, the experimental results of the proposed method are better.
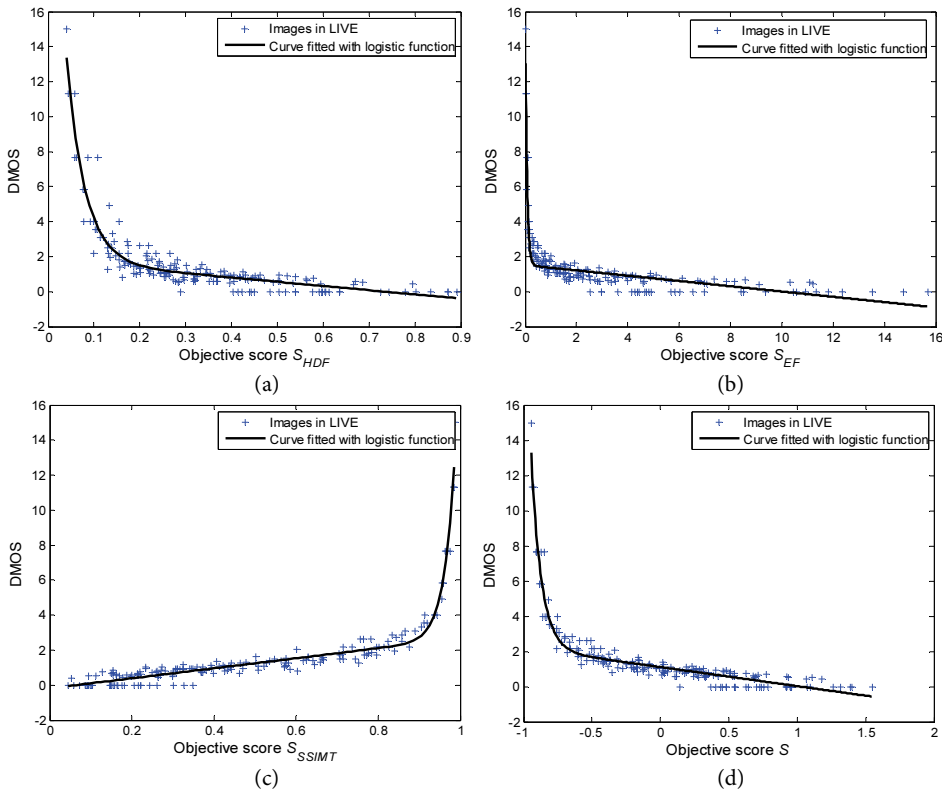

Fig. 9. Scatter plots of subjective DMOS against predicted scores obtained by the proposed method in LIVE database: (a) objective score S_{HDF}, (b) objective score S_{EF}, (c) objective score S_{SSIMT}, and (d) objective score S.

Fig. 9 gives the scatter plots of subjective DMOS against predicted scores obtained by our proposed method in LIVE database. Table 3 shows the experimental results of blurred images in LIVE for S_{HDF}, S_{EF}, S_{SSIMT}, and S in terms of SROCC, KROCC, PLCC, and RMSE.

Table 3. Experimental results of images in LIVE database for the proposed method

Metrics	S_{HDF}	S_{EF}	S_{SSIMT}	S
SROCC	0.8841	0.9122	0.9378	0.9374
KROCC	0.7157	0.7606	0.8064	0.7993
PLCC	0.9416	0.9545	0.9811	0.9616
RMSE	0.6934	0.6139	0.3984	0.4870

The overall performance of our proposed method is evaluated based on the four image quality databases. For comparison, we also compared with previously proposed methods including FR methods and NR methods. The FR methods include PSNR and SSIM [4]. The NR methods include JNB [14] and CPBD [15]. Fig. 10 gives the scatter plots of subjective MOS/DMOS scores against predicted scores obtained by the proposed method on four databases. Table 4 summarizes the experimental results of our proposed method with different image quality assessment methods in terms of SROCC, KROCC, PLCC, and RMSE.
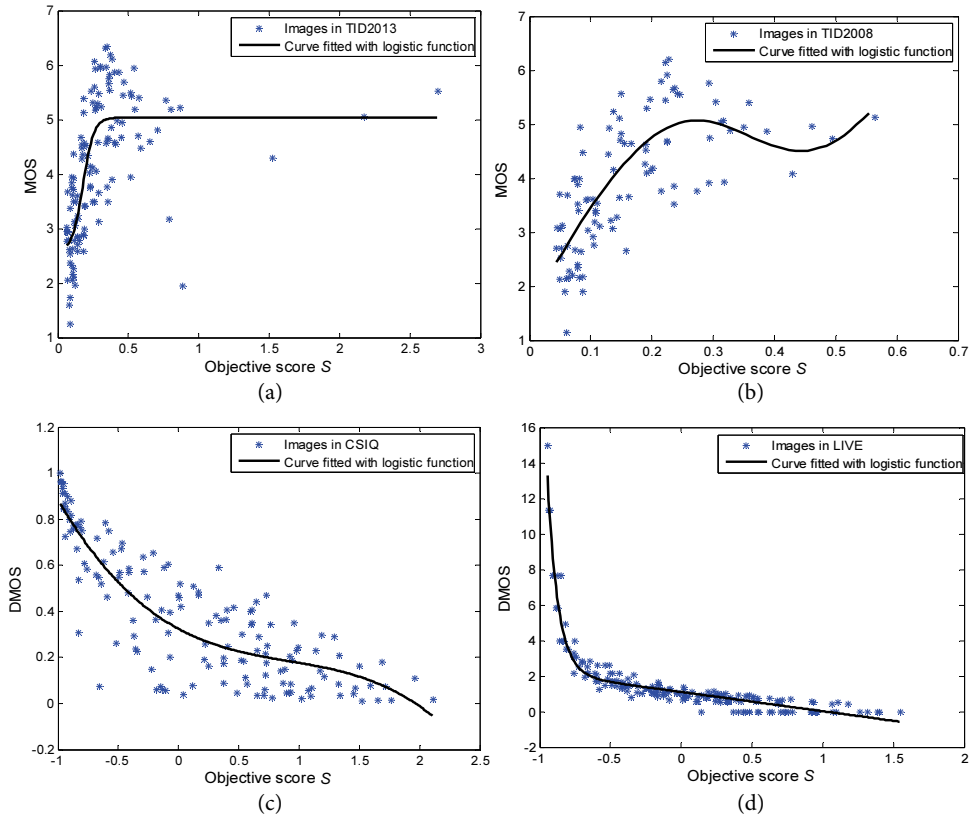

Fig. 10. Scatter plots of subjective MOS/DMOS against predicted scores obtained by the proposed method on four databases: (a) TID2013, (b) TID2008, (c) CSIQ, and (d) LIVE.

Table 4. Summary of experimental results for the proposed method and other existing image quality metrics

Datasets	Metrics	SROCC	KROCC	PLCC	RMSE
TID2013	PSNR	0.9149	0.7884	0.9137	0.5071
	SSIM	0.9629	0.8285	0.9577	0.3592
	JNB	0.6902	0.5137	0.7114	0.8770
	CPBD	0.8515	0.6462	0.8553	0.6466
	Proposed	0.6888	0.5259	0.7492	0.8266
TID2008	PSNR	0.8697	0.7332	0.8729	0.5726
	SSIM	0.9386	0.7862	0.9338	0.4200
	JNB	0.6667	0.4951	0.6931	0.8459
	CPBD	0.8414	0.6301	0.8237	0.6654
	Proposed	0.7392	0.5208	0.7582	0.7560
CSIQ	PSNR	0.9291	0.7543	0.9252	0.1087
	SSIM	0.9245	0.7665	0.9005	0.1246
	JNB	0.7624	0.5976	0.8061	0.1696
	CPBD	0.8853	0.7090	0.8822	0.1349
	Proposed	0.8156	0.6406	0.8615	0.1454
LIVE	PSNR	0.7832	0.5847	0.7835	11.478
	SSIM	0.8944	0.7136	0.8743	8.9643
	JNB	0.7871	0.6069	0.8160	10.677
	CPBD	0.9186	0.7634	0.8953	8.2263
	Proposed	0.9374	0.7993	0.9616	0.4870

From Fig. 10 and Table 4, it can be seen that our proposed method has the best performance for LIVE database among four databases. Compared with the five different image quality assessment methods, our proposed method in LIVE database also achieves the best experimental results. In TID2013, TID2008, our proposed method achieves similar results compared with JNB and CPBD. In CSIQ, our proposed method obtains slightly better experimental results compared with JNB and CPBD. From all the experimental results, we can find that our proposed method can achieve better performance in terms of monotonicity and prediction accuracy.

5. Conclusions

We proposed a novel blind quality assessment scheme for Gaussian blurred images. The novel method is based on the fact that images with different blur degree will have different changes through the same blur. This discrimination is described from three aspects: color, edge, and structure. The nonlinear fitting gives good consistency with MOS/DMOS scores. We use the visual saliency to make experimental results consistent with human visual system, and make full use of good characteristics of SSIM and structure tensor. Extensive experiments show that our proposed method achieves better performance, especially in LIVE database. We can use it to test image dehazing algorithms because dehazed images have the similar features of blurred images. Given the phenomenon that the blur is one

of the distortions of the JPEG compressed images (another is blocking artifacts), we can research this scheme for JPEG compressed images further.

Acknowledgement

References

[1] L. J. Karam, T. Ebrahimi, S. S. Hemami, T. N. Pappas, R. J. Safranek, Z. Wang, and A. B. Watson, "Introduction to the issue on visual media quality assessment," *IEEE Journal of Selected Topics in Signal Processing*, vol. 3, no. 2, pp. 189-192, 2009.

[2] S. Bekkouch and K. M. Faraoun, "Robust and reversible image watermarking scheme using combined DCT-DWT-SVD transforms," *Journal of Information Processing Systems*, vol. 11, no. 3, pp. 406-420, 2015.

[3] J. Agarwal and S. S. Bedi, "Implementation of hybrid image fusion technique for feature enhancement in medical diagnosis," *Human-Centric Computing and Information Sciences*, vol. 5, no. 3, pp. 1-17, 2015.

[4] Z. Wang, A. C. Bovik, H. R. Sheikh, and E. P. Simoncelli, "Image quality assessment: from error visibility to structural similarity," *IEEE Transactions on Image Processing*, vol. 13, vo. 4, pp. 600-612, 2004.

[5] S. Maksimovic-Moicevic, Z. Lukac, and M. Temerinac, "Edge-texture 2D image quality metrics suitable for evaluation of image interpolation algorithms," *Computer Science and Information Systems*, vol. 12, no. 2, pp. 405-425, 2015.

[6] J. J. Wu, W. S. Lin, G. M. Shi, and A. M. Liu, "Reduced-reference image quality assessment with visual information fidelity," *IEEE Transactions on Multimedia*, vol. 15, no. 7, pp. 1700-1705, 2013.

[7] Y. M. Fang, K. D. Ma, Z. Wang, W. S. Lin, Z. J. Fang, and G. T. Zhai, "No-reference quality assessment of contrast-distorted images based on natural scene statistics," *IEEE Signal Processing Letters*, vol. 22, no. 7, pp. 838-842, 2015.

[8] A. Mittal, A. K. Moorthy, and A. C. Bovik, "No-reference image quality assessment in the spatial domain," *IEEE Transactions on Image Processing*, vol. 21, no. 12, pp. 4695-4708, 2012.

[9] M. A. Saad, A. C. Bovik, and C. Charrier, "Blind image quality assessment: a natural scene statistics approach in the DCT domain," *IEEE Transactions on Image Processing*, vol. 21, no. 8, pp. 3339-3352, 2012.

[10] W. F. Xue, X. Q. Mou, L. Zhang, A. C. Bovik, and X. C. Feng, "Blind image quality assessment using joint statistics of gradient magnitude and Laplacian features," *IEEE Transactions on Image Processing*, vol. 23, no. 11, pp. 4850-4862, 2014.

[11] P. Marziliano, F. Dufaux, S. Winkler, and T. Ebrahimi, "Perceptual blur and ringing metrics: application to JPEG2000," *Signal Processing: Image Communication*, vol. 19, no. 2, pp. 163-172, 2004.

[12] G. Cao, Y. Zhao, and R. R. Ni, "Edge-based blur metric for tamper detection," *Journal of Information Hiding and Multimedia Signal Processing*, vol. 1, no. 1, pp. 20-27, 2010.

[13] C. Feichtenhofer, H. Fassold, and P. Schallauer, "A perceptual image sharpness metric based on local edge gradient analysis," *IEEE Signal Processing Letters*, vol. 20, no. 4, pp. 379-382, 2013.

[14] R. Ferzli and L. J. Karam, "A no-reference objective image sharpness metric based on the notion of just noticeable blur (JNB)," *IEEE Transactions on Image Processing*, vol. 18, no. 4, pp. 717-728, 2009.

[15] N. D. Narvekar and L. J. Karam, "A no-reference image blur metric based on the cumulative probability of blur detection (CPBD)," *IEEE Transactions on Image Processing*, vol. 20, no. 9, pp. 2678-2683, 2011.

[16] R. Hassen, Z. Wang, and M. Salama, "No-reference image sharpness assessment based on local phase coherence measurement," in *Proceedings of the IEEE International Conference on Acoustics, Speech, and Signal Processing*, Dallas, TX, USA, 2010, pp. 2434-2437.

[17] C. T. Vu, T. D. Phan, and D. M. Chandler, "S$_3$: a spectral and spatial measure of local perceived sharpness in natural images," *IEEE Transactions on Image Processing*, vol. 21, no. 3, pp. 934-945, 2012.

[18] T. Brox, J. Weickert, B. Burgeth, and P. Mrazek, "Nonlinear structure tensors," *Image and Vision Computing*, vol. 24, no. 1, pp. 41-55, 2006.

[19] H. R. Sheikh, Z. Wang, L. Cormack, and A. C. Bovik, "LIVE Image Quality Assessment Database Release 2" [Online]. Available: http://live.ece.utexas.edu/research/quality.

[20] X. D. Hou, J. Harel, and C. Koch, "Image signature: highlighting sparse salient regions," *IEEE Transactions on Pattern Analysis and Machine Intelligence*, vol. 34, no. 1, pp. 194-201, 2012.

[21] L. Zhang, Y. Shen, and H. Y. Li, "VSI: a visual saliency-induced index for perceptual image quality assessment," *IEEE Transactions on Image Processing*, vol. 23, no. 10, pp. 4270-4281, 2014.

[22] L. Zhang, Z. Y. Gu, and H. Y. Li, "SDSP: a novel saliency detection method by combining simple priors," in *Proceedings of the 20th IEEE International Conference on Image Processing*, Melbourne, Australia, 2013, pp. 171-175.

[23] N. Ponomarenko, L. N. Jin, O. Ieremeiev, V. Lukin, K. Egiazarian, J. Astola, et al., "Image database TID2013: peculiarities, results and perspectives," *Signal Processing: Image Communication*, vol. 30, pp. 57-77, 2015.

[24] N. Ponomarenko, V. Lukin, A. Zelensky, K. Egiazarian, J. Astola, M. Carli, and F. Battisti, "TID2008 - a database for evaluation of full-reference visual quality assessment metrics," *Advances of Modern Radioelectronics*, vol. 10, no. 4, pp. 30-45, 2009.

[25] E. C. Larson and D. M. Chandler, "Most apparent distortion: full-reference image quality assessment and the role of strategy," *Journal of Electronic Imaging*, vol. 19, no. 1, pp. 1-21, 2010.

[26] H. R. Sheikh, M. F. Sabir, and A. C. Bovik, "A statistical evaluation of recent full reference image quality assessment algorithms," *IEEE Transactions on Image Processing*, vol. 15, no. 11, pp. 3440-3451, 2006.

Liping Wang http://orcid.org/0000-0003-0686-3862

She was born in Shandong province, China, in 1990. She received her B.E. degree in communication engineering from Shandong University, Weihai, China, in 2014. She is currently pursuing her M.E. degree in signal and information processing at Shandong University, China. Her current research interests include image dehazing, image deblocking, and blind image quality assessment.

Chengyou Wang http://orcid.org/0000-0002-0901-2492

He was born in Shandong province, China, in 1979. He received his B.E. degree in electronic information science and technology from Yantai University, China, in 2004, and his M.E. and Ph.D. degrees in signal and information processing from Tianjin University, China, in 2007 and 2010, respectively. He is currently an associate professor and supervisor of postgraduate students with Shandong University, Weihai, China. His current research interests include transform coding, digital watermarking, image authentication, and blind image quality assessment.

Xiao Zhou http://orcid.org/0000-0002-1331-7379

She was born in Shandong province, China, in 1982. She received her B.E. degree in automation from Nanjing University of Posts and Telecommunications, China, in 2003; her M.E. degree in information and communication engineering from Inha University, Korea, in 2005; and her Ph.D. degree in information and communication engineering from Tsinghua University, China, in 2013. She is currently a lecturer and supervisor of postgraduate students with Shandong University, Weihai, China. Her current research interests include wireless communication technology, image communication, and computer vision.